The EMBO Journal (2012) 31, 1147–1159 | © 2012 European Molecular Biology Organization | All Rights Reserved 0261-4189/12
www.embojournal.org

THE EMBO JOURNAL

Ablation of Rassf2 induces bone defects and subsequent haematopoietic anomalies in mice

Hoogeun Song[1,8], Hyunsoo Kim[2,8], Kyunghee Lee[2], Da-Hye Lee[1], Tae-Shin Kim[1], Ji Yun Song[1], Dongjun Lee[1], Dongwook Choi[3], Chang-Yong Ko[4], Han-Sung Kim[4], Hong-In Shin[5], Juhyun Choi[6], Heedong Park[7], Chankyu Park[3], Daewon Jeong[2,*] and Dae-Sik Lim[1,*]

[1]Department of Biological Sciences, National Creative Research Initiatives Center, Graduate School of Nanoscience and Technology (WCU), Korea Advanced Institute of Science and Technology, Daejeon, Korea, [2]Department of Microbiology, Aging-Associated Vascular Disease Research Center, Yeungnam University College of Medicine, Daegu, Korea, [3]Department of Biological Sciences, Korea Advanced Institute of Science and Technology, Daejeon, Korea, [4]Department of Biomedical Engineering, College of Health Science, Institute of Medical Engineering, Yonsei University, Wonju, Korea, [5]IHBR, Department of Oral Pathology, School of Dentistry, Kyungpook National University, Daegu, Korea, [6]Biosimilar Group, Research and Development Park, LG Life Sciences, Daejeon, Korea and [7]Department of Pharmacology, Research and Development Park, LG Life Sciences, Daejeon, Korea

RASSF2 belongs to the Ras-association domain family (RASSF) of proteins, which may be involved in the Hippo signalling pathway. However, the role of RASSF2 *in vivo* is unknown. Here, we show that *Rassf2* knockout mice manifest a multisystemic phenotype including haematopoietic anomalies and defects in bone remodelling. Bone marrow (BM) transplantation showed that *Rassf2*$^{-/-}$ BM cells had a normal haematopoietic reconstitution activity, indicating no intrinsic haematopoietic defects. Notably, *in vitro* differentiation studies revealed that ablation of *Rassf2* suppressed osteoblastogenesis but promoted osteoclastogenesis. Co-culture experiments showed that an intrinsic defect in osteoblast differentiation from *Rassf2*$^{-/-}$ osteoblast precursors likely leads to both haematopoiesis and osteoclast defects in *Rassf2*$^{-/-}$ mice. Moreover, *Rassf2* deficiency resulted in hyperactivation of nuclear factor (NF)-κB during both osteoclast and osteoblast differentiation. RASSF2 associated with IκB kinase (IKK) α and β forms, and suppressed IKK activity. Introduction of either RASSF2 or a dominant-negative form of IKK into *Rassf2*$^{-/-}$ osteoclast or osteoblast precursors inhibited NF-κB hyperactivation and normalized osteoclast and osteoblast differentiation. These observations indicate that RASSF2 regulates osteoblast and osteoclast differentiation by inhibiting NF-κB signalling.

The EMBO Journal (2012) **31,** 1147–1159. doi:10.1038/emboj.2011.480; Published online 6 January 2012
Subject Categories: signal transduction; development
Keywords: bone remodelling; Hippo pathway; osteoblastogenesis; osteoclastogenesis; RASSF2

Introduction

RASSF2 is a member of the RASSF (Ras-association domain family) protein family (which has 10 members, RASSF1–10) and induces cell-cycle arrest and apoptosis (Cooper *et al*, 2008; Imai *et al*, 2008; Maruyama *et al*, 2008). RASSF2 binds directly to K-Ras in a GTP-dependent manner via the RA (Ras-association) domain (Vos *et al*, 2003). *RASSF2* is often inactivated in several types of tumours including breast, lung, and gastric cancers, and hepatocellular carcinoma (Cooper *et al*, 2008; Maruyama *et al*, 2008; Ren *et al*, 2009). Global gene expression profiling analyses of RASSF2-overexpressing cancer cells have suggested that RASSF2 inhibits expression of genes involved in the immune response, haematologic development, and tumourigenesis, as well as genes activating nuclear factor (NF)-κB signalling (Imai *et al*, 2008; Maruyama *et al*, 2008). RASSF2 has been shown to associate with and stabilize MST1 and MST2 via the SARAH (Sav/RASSF/Hpo) domain (Cooper *et al*, 2009), raising the possibility that RASSF2 plays a role in the Hippo signalling pathway. The latter pathway, including Hpo (the *Drosophila* homologue of MST), Sav (the *Drosophila* homologue of WW45), Wts (the *Drosophila* homologue of LATS), Yki (the *Drosophila* homologue of YAP), and dRASSF, has been implicated in restriction of cell proliferation and in control of organ size (Zhao *et al*, 2008; Pan, 2010; Sudol and Harvey, 2010). Genetic ablation of Hippo components in mammals, thus *WW45*, *Lats2*, or *YAP* knockout or *Mst1* and *Mst2* double knockout in mice, resulted in embryonic lethality. This indicates that the Hippo pathway plays a crucial role in development (McPherson *et al*, 2004; Morin-Kensicki *et al*, 2006; Lee *et al*, 2008; Oh *et al*, 2009). In addition, transgenic overexpression of YAP (Camargo *et al*, 2007; Dong *et al*, 2007) or liver-specific deletion of *WW45* or *Mst1/2* (Zhou *et al*, 2009; Lee *et al*, 2010; Lu *et al*, 2010; Song *et al*, 2010a) induces hepatocellular carcinoma. Turning to the RASSF protein family, *Rassf1a*-deficient mice exhibited spontaneous tumourigenesis, including development of lymphomas and lung adenomas, when at an advanced age (Tommasi *et al*, 2005; van der Weyden *et al*, 2005). Moreover, mice deficient in *Nore1b* (an isoform of RASSF5; also known as RAPL) exhibited impaired lymphocyte trafficking and lymphoid organ abnormalities (Katagiri *et al*, 2004). *Rassf5*-null mice were significantly more resistant (compared with wild-type

*Corresponding authors. D Jeong, Department of Microbiology, Aging-Associated Vascular Disease Research Center, Yeungnam University College of Medicine, Daegu 705-717, Korea. Tel.: +82 53 620 4365; Fax: +82 53 653 6628; E-mail: dwjeong@ynu.ac.kr or D-S Lim, Department of Biological Sciences, National Creative Research Initiatives Center, Graduate School of Nanoscience and Technology (WCU), Korea Advanced Institute of Science and Technology, Daejeon 305-701, Korea. Tel.: +82 42 350 2635; Fax: +82 42 350 2610; E-mail: daesiklim@kaist.ac.kr
[8]These authors contributed equally to this work

Received: 30 May 2011; accepted: 6 December 2011; published online: 6 January 2012

(WT) mice) to TNFα-induced apoptosis and failed to activate Mst1 *in vivo* (Park *et al*, 2010). However, animal models allowing investigation of the *in vivo* function of RASSF2 have not yet been developed.

The immune and skeletal systems are closely inter-related (Walsh *et al*, 2006; Takayanagi, 2007). A number of regulatory factors, including immunoregulatory cytokines and signalling molecules, are expressed by both bone and immune system cells. Haematopoietic stem cells (HSCs) are maintained in the bone marrow (BM), and bone provides a microenvironment for immune cell development from HSCs. Bone is continuously remodelled by the opposing processes of osteoblast-mediated bone formation and osteoclast-induced bone resorption. Mesenchymal stem cell (MSC)-derived osteoblasts and HSC-derived osteoclasts can communicate via paracrine factors, including receptor activator of NF-κB ligand (RANKL) and macrophage colony-stimulating factor (M-CSF). Interaction between RANKL from osteoblasts and RANK on osteoclast precursors is essential for osteoclast differentiation (Matsuo and Irie, 2008). In addition, osteoblasts produce haematopoietic factors regulating the maintenance of HSCs; these factors include osteopontin and angiopoietin (Arai *et al*, 2004; Nilsson *et al*, 2005; Stier *et al*, 2005). Previous studies have revealed that impaired bone development caused by osteoblastic defects can induce defective haematopoiesis in mice (Calvi *et al*, 2003; Zhang *et al*, 2003; Visnjic *et al*, 2004).

In the present study, we have developed, for the first time, a mouse model that reveals the physiological role of RASSF2. *Rassf2*$^{-/-}$ mice exhibited systematic haematopoietic anomalies, which may be attributable to bone microenvironmental changes. *Rassf2*-deficient animals exhibited a severe osteoporotic phenotype caused by defects in both osteoclast and osteoblast differentiation. We have also shown that RASSF2 attenuates osteoclastogenesis and stimulates osteoblastogenesis *in vitro* by inhibiting the NF-κB signalling that is critical for maintenance of bone remodelling.

Results

Loss of Rassf2 leads to growth retardation, systemic lymphopenia, and development of a severe osteoporotic phenotype

To define the role of RASSF2 in mammals, *Rassf2*$^{-/-}$ mice were generated (Figure 1A; Supplementary Figure S1A). Rassf2 protein was detected in all normal mouse tissues examined, including the liver, brain, lung, BM, lymph node (LN), spleen, and testis, and the absence of such expression was confirmed in *Rassf2*$^{-/-}$ mice (Supplementary Figure S1B). Offspring of *Rassf2*$^{+/-}$ intercrosses were born in the expected Mendelian ratio and appeared to develop normally for 2 weeks after birth. However, *Rassf2*$^{-/-}$ mice exhibited growth retardation commencing at 2 weeks of age and postnatal mortality was evident at ∼4 weeks of age (Figure 1B; Supplementary Figure S1C). To identify the phenotypic defects of *Rassf2*$^{-/-}$ mice, we first performed histological analysis of representative tissues isolated from WT and mutant animals at 3 weeks of age. Most *Rassf2*$^{-/-}$ tissues, including the brain, heart, lung, intestine, and kidney, were normal (thus, similar to WT tissue) at this age, but the thymus, spleen, BM, and liver were not. *Rassf2*$^{-/-}$ mice exhibited thinning of cortical thymic epithelial cells, mild congestion in the red pulp of the spleen, decreased cellularity of the BM, and mild periportal fibrosis of the liver (Supplementary Figure S2A). Moreover, *Rassf2*$^{-/-}$ animals also exhibited marked abnormalities in bone development, including decreases in bone mass and the extent of trabecular bone (Figure 2A and B). Together, the data showed that *Rassf2*$^{-/-}$ mice developed multisystemic abnormalities.

We first addressed abnormalities of haematopoiesis in such animals. We found that total cell numbers in the thymus, spleen, and BM, as well as those of peripheral blood leukocytes and red blood cells, were greatly reduced in mutant animals (Supplementary Figure S2B and data not shown). *Rassf2*$^{-/-}$ mice also had reduced numbers of T, B, and myeloid cells in the thymus, spleen, and BM (Figure 1C; Supplementary Figure S2C). In addition, the thymus and spleen weights of *Rassf2*$^{-/-}$ mice were markedly lower than were those of WT littermates. However, other organs, including the liver, were unaltered in mutant animals, indicating that the observed hypotrophy was specific to lymphoid organs (Supplementary Figure S2D). Because we had observed an overall reduction in lymphocyte number and histological anomalies in *Rassf2*$^{-/-}$ lymphoid organs, we next investigated whether the lymphopenic phenotype of mutant mice was caused by impaired haematopoiesis in adulthood. To this end, we analysed HSC-enriched Lin^{-}Sca1^{+}c-Kit^{+} (LSK) cells as well as Lin^{-}Sca1^{-}c-Kit^{+} myeloid progenitor (MP) cells. The proportional contributions of LSK and MP cells to total BM cells were markedly decreased in *Rassf2*$^{-/-}$ mice compared with WT controls (Figure 1D). Consistent with this finding, a colony-forming cell assay showed that the population of committed haematopoietic progenitor cells was reduced in *Rassf2*$^{-/-}$ mice (Supplementary Figure S2E). Using competitive BM transplantation, we first investigated whether the reduced populations of HSCs, haematopoietic progenitors, and leukocytes in mutant animals were due to an intrinsic defect in the repopulation capacity of HSCs. CD45.2^{+} BM cells from WT or *Rassf2*$^{-/-}$ mice were mixed with CD45.1^{+} control BM cells from WT competitor animals in a 2:1 ratio and then transplanted into lethally irradiated CD45.1^{+} recipient mice. Unexpectedly, haematopoietic reconstitution by CD45.2^{+} donor-derived cells at 12 weeks after transplantation did not differ substantially compared with cells from WT and mutant donors (Figure 1E; Supplementary Figure S3), indicating that transplanted mutant BM cells exhibited normal haematopoietic developmental capacity. However, we could not transplant CD45.1^{+} control BM cells to *Rassf2*$^{-/-}$ mice because the animals died soon after birth. Together, the results indicated that the impaired haematopoiesis of *Rassf2*$^{-/-}$ mice was probably not attributable to an intrinsic developmental defect of HSCs.

RASSF2 regulates postnatal bone development

Since it is known that the activation of osteoblasts in the BM regulates the HSC niche (Calvi *et al*, 2003), we then focused on bone microenvironment changes that might explain the haematopoietic defects and growth retardation of *Rassf2*$^{-/-}$ mice. High-resolution microcomputed tomography investigating bone microstructure in *Rassf2*$^{-/-}$ mice revealed a pronounced osteoporotic phenotype characterized by marked decreases in trabecular bone volume, bone mineral density, and the number and thickness of trabeculae, as well

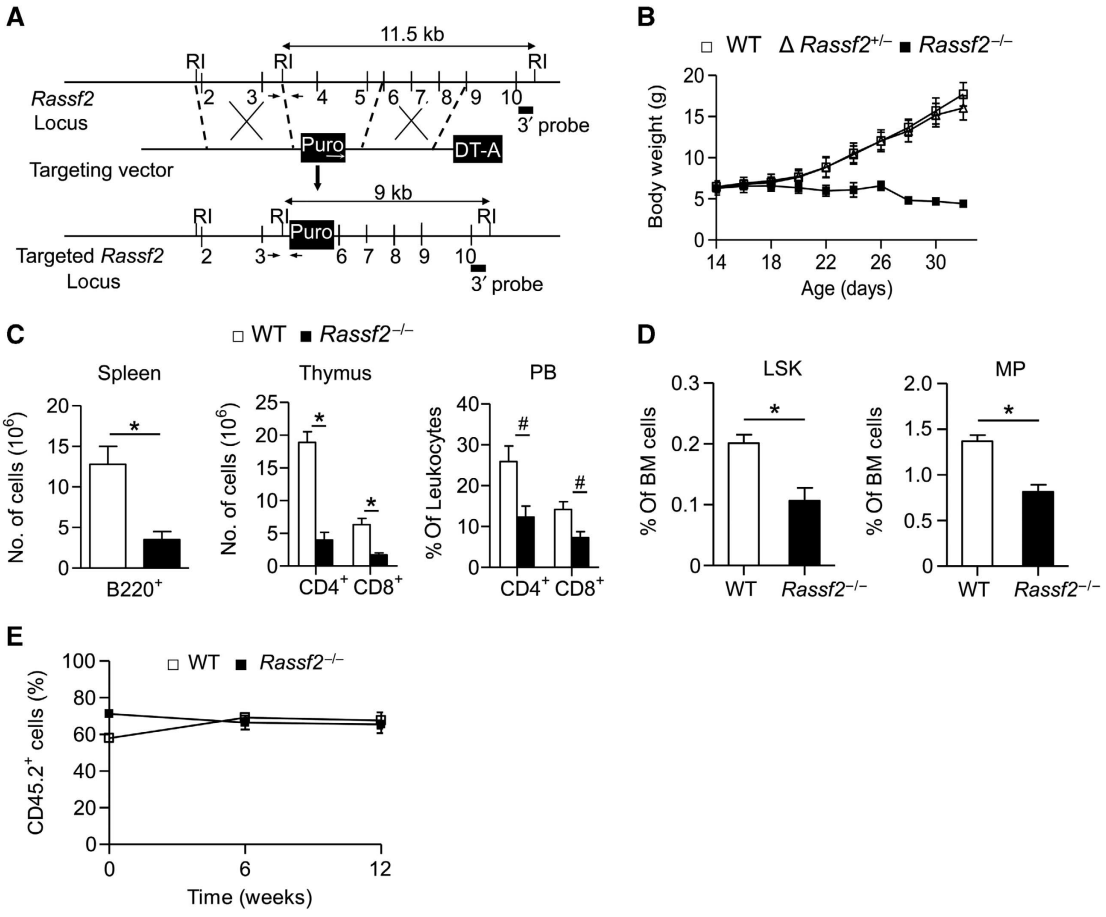

Figure 1 Targeted disruption of *Rassf2* results in growth retardation and non-cell-autonomous defects in haematopoiesis. (**A**) Targeting strategy for *Rassf2* knockout. RI, *Eco*RI; Puro, puromycin-resistance gene; DT-A, diphtheria toxin A gene. Numbered vertical lines indicate *Rassf2* exons, and small arrows denote 5′ and 3′ genotyping site sequences. The 3′ probe used in Southern blot analysis is indicated. (**B**) Growth curve of WT, heterozygous, and *Rassf2*$^{-/-}$ mice; data are mean values ± s.d. ($n = 15$–27). (**C**) Numbers of B cells (B220$^+$) in the spleen and T cells (CD4$^+$ or CD8$^+$) in the thymus and peripheral blood (PB) of WT and *Rassf2*$^{-/-}$ mice at 3–4 weeks of age; data are mean values ± s.e.m. ($n = 4$ or 5, $^*P < 0.01$, $^{\#}P < 0.05$). (**D**) Percentages of LSK and MP cells among BM cells from 3- to 4-week-old WT and *Rassf2*$^{-/-}$ mice; data are mean values ± s.e.m. ($n = 5$, $^*P < 0.01$). (**E**) The percentage contributions of CD45.2$^+$ leukocytes to donor-derived peripheral blood leukocytes were determined by flow cytometry at the indicated times after transplantation; data are mean values ± s.e.m. (WT mice, $n = 4$; *Rassf2*$^{-/-}$ mice, $n = 5$).

as an associated increase in trabecular bone separation (Figure 2A). Whereas WT littermates showed a gradual increase in bone mass after birth, *Rassf2*$^{-/-}$ mice did not show such an increase between 14 and 24 days of age (Figure 2A); this was coincident with the period of growth retardation in mutant animals (Figure 1B). The numbers of bone-forming osteoblasts and bone-degrading osteoclasts in trabecular bone tissue, as visualized by haematoxylin–eosin (H&E) and tartrate-resistant acid phosphatase (TRAP) staining, respectively, were also significantly decreased in *Rassf2*$^{-/-}$ mice (Figure 2B). We next directly measured the mineral apposition rate (MAR) and found that this value was markedly reduced in mutant animals (Figure 2C). We also noted that *Rassf2*$^{-/-}$ mice showed decreased levels of serum RANKL and M-CSF (Figure 2D); these effectors are produced principally by cells of the osteoblast lineage and stimulate osteoclast formation. In addition, levels of serum and urine type 1 collagen crosslinked telopeptide (CTX), a bone resorption marker, were reduced in mutant animals (Figure 2E). These results indicated that the osteoporotic phenotype of *Rassf2*$^{-/-}$ mice might be attributable to reduced bone turnover caused by impairment of osteoblast and osteoclast formation, and that RASSF2 might play a role in normal bone remodelling in the early stage of postnatal development.

RASSF2 regulates osteoblast and osteoclast differentiation

To identify the intrinsic defects of osteoblasts and osteoclasts in *Rassf2*$^{-/-}$ mice, we examined, first, osteoblastogenesis from calvarial osteoblast precursors cultured in osteogenic medium, and second, osteoclastogenesis from BM-derived macrophages (BMMs) cultured in conditioned medium containing RANKL and M-CSF. Surprisingly, *Rassf2*$^{-/-}$ osteoblast precursors manifested a reduced extent of osteoblast differentiation without affecting the formation of osteoblast progenitors of MSC origin (Figure 3A; Supplementary Figure S4). In agreement with these findings, global gene expression profiling analyses also revealed that expression levels of *Rassf2*$^{-/-}$ osteoblast markers were reduced compared with WT cells (Figure 3B). We further confirmed downregulation of markers such as *Alp*, *Bmp2*, *Bmp4*, *Rankl*, *Csf1*, *Sp7*, *Bglap1*, *Spp1*, Fra-1, and Runx2 in *Rassf2*$^{-/-}$ osteoblast

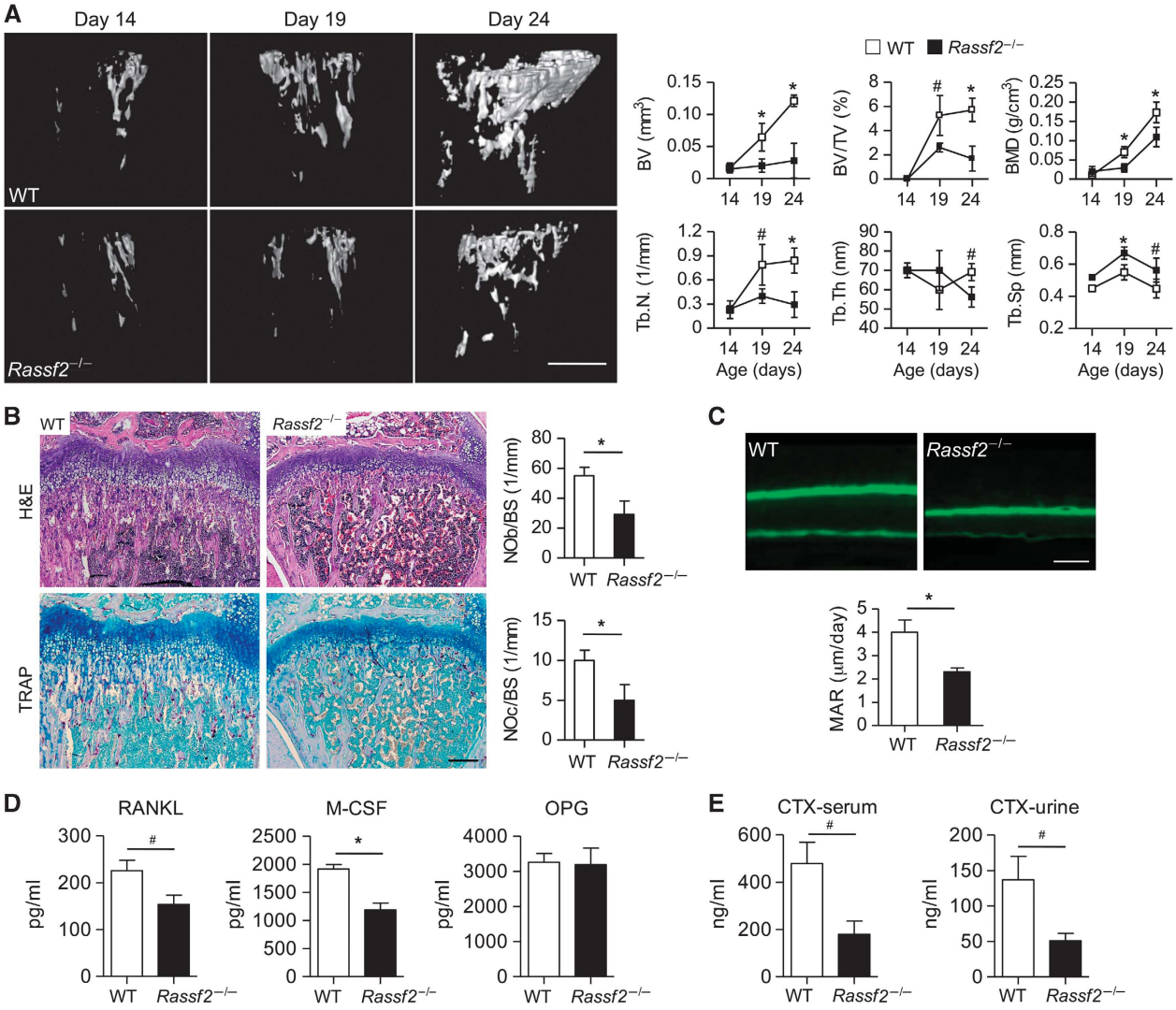

Figure 2 *Rassf2* deficiency deregulates bone remodelling. (**A**) Microcomputed tomography of the tibiae of WT and *Rassf2*$^{-/-}$ mice showing postnatal skeletal development. Representative images are shown in the left panels (scale bar, 0.5 mm). Quantitative data (mean values ± s.d.; $n=4$–8, $^{*}P<0.01$, $^{\#}P<0.05$) for bone volume (BV), bone volume per unit of tissue volume (BV/TV), bone mineral density (BMD), trabecular number (Tb.N), trabecular thickness (Tb.Th), and trabecular separation (Tb.Sp) are shown in the right panels. (**B**) Tibial sections from 3-week-old WT and *Rassf2*$^{-/-}$ mice were stained with H&E or for TRAP (left panels); scale bar, 200 μm. The numbers of osteoblasts per bone surface (NOb/BS) and osteoclasts per bone surface (NOc/BS) were determined (right panels); data are mean values ± s.d. ($n=4$–8, $^{*}P<0.01$). (**C**) Analysis of trabecular bone surface dynamics in 3-week-old *Rassf2*$^{-/-}$ and WT mice using the calcein double-labelling method. Representative images are shown in the upper panels (scale bar, 10 μm) and MARs are quantitated in the lower panels (mean values ± s.d.; $n=3$, $^{*}P<0.01$). (**D**) Serum M-CSF, RANKL, and OPG levels were measured by ELISA; data are mean values ± s.e.m. ($n=4$, $^{*}P<0.01$, $^{\#}P<0.05$). (**E**) Serum and urine type 1 collagen CTX levels were analysed by ELISA; data are mean values ± s.e.m. ($n=4$, $^{\#}P<0.05$).

precursors using RT–PCR (polymerase chain reaction), real-time PCR, or immunoblot (IB) analysis during osteoblast differentiation (Figure 3C and D; Supplementary Figure S5). In contrast, BMMs prepared from *Rassf2*$^{-/-}$ mice manifested enhanced formation of TRAP-positive multinucleated cells (TRAP^{+} MNCs) and increased pit formation on dentine slices compared with the corresponding WT cells (Figure 3E and F), indicating that RASSF2 functions as an inhibitor of osteoclast formation and function. Global gene expression profiling analyses also revealed that expression levels of osteoclast differentiation markers were increased in *Rassf2*$^{-/-}$ osteoclasts (Supplementary Figure S6A). These results were further confirmed by RT–PCR or IB analysis during osteoclast differentiation, which showed upregulation of markers such as *Acp5*, *Ctsk*, *Oscar*, c-Src, c-Fos, and NFATc1 in *Rassf2*$^{-/-}$ BMMs (Supplementary Figure S6B and C). Notably, the numbers of osteoblasts and osteoclasts in bone were also significantly decreased in *Rassf2*$^{-/-}$ mice (Figure 2B). Therefore, we next attempted to explain the inconsistency in osteoclast formation from *Rassf2*$^{-/-}$ cells *in vivo* and *in vitro*. To this end, we co-cultured BMMs and primary calvarial osteoblasts to examine osteoclastogenesis. Co-culture of WT or *Rassf2*$^{-/-}$ BMMs with WT or *Rassf2*$^{-/-}$ primary osteoblasts in conditioned medium, which can induce expression of RANKL and M-CSF by osteoblast precursors and eventually give rise to osteoclastogenesis, revealed that WT osteoblasts did indeed induce formation of more osteoclasts from *Rassf2*$^{-/-}$ BMMs than from WT BMMs (Figure 3G). However, *Rassf2*$^{-/-}$ osteoblast precursors eventually failed to induce osteoclast formation from WT or *Rassf2*$^{-/-}$

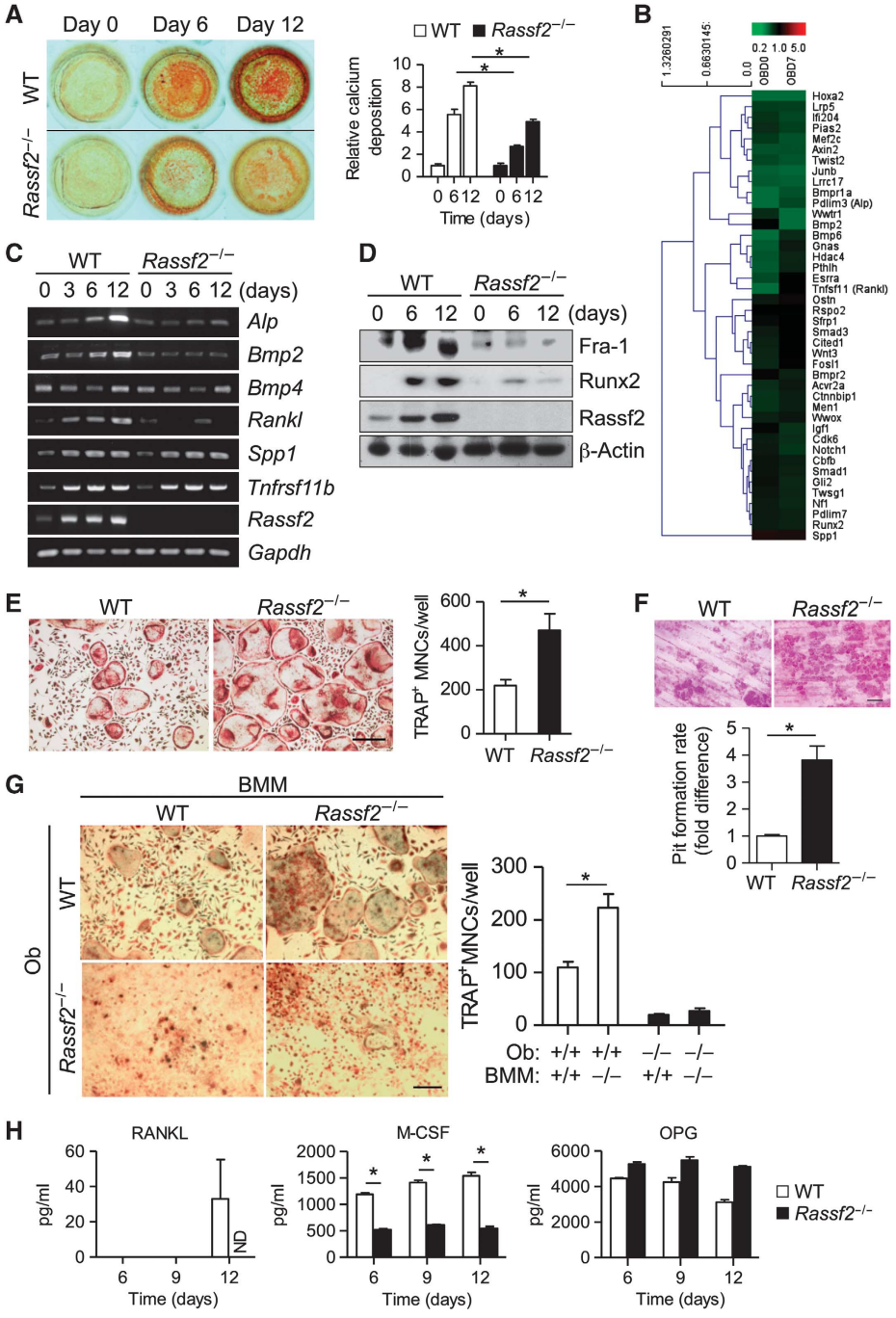

Figure 3 RASSF2 promotes osteoblast differentiation and inhibits osteoclast differentiation. (**A**) Calcium deposition during differentiation of osteoblasts from calvarial osteoblast precursors isolated from *Rassf2*$^{-/-}$ and WT littermates. Representative alizarin red S staining images of cultures on days 0, 6, and 12 are shown on the left, and quantitative data appear on the right (the figures are expressed relative to the values for WT cells on day 0, and are mean values ± s.d.; $n=4$, $^{*}P<0.01$). (**B**) Global gene expression profiling of WT and *Rassf2*$^{-/-}$ osteoblasts. Expression of marker genes for osteoblast differentiation (biological process GO 0001649) was analysed in *Rassf2*$^{-/-}$ osteoblast precursors both before (day 0, OBD0) and during differentiation into osteoblasts (day 7, OBD7), and compared with that of WT cells. Data are shown relative to expression levels in the latter type of cells. (**C**, **D**) RT–PCR analysis of the expression of osteoblast differentiation marker genes and *Rassf2* (**C**), and IB analysis of osteoblast differentiation marker proteins and Rassf2 (**D**), during osteoblastogenesis in osteogenic medium of calvarial osteoblast precursors isolated from *Rassf2*$^{-/-}$ and WT mice. *Gapdh* and β-actin were used as controls in either analysis. (**E**) Osteoclast differentiation from BMMs prepared from *Rassf2*$^{-/-}$ and WT littermates. TRAP-positive multinucleated osteoclasts (TRAP^{+} MNCs) after culture for 4 days in the presence of RANKL and M-CSF are shown on the left (scale bar, 100 μm), and the numbers of TRAP^{+} MNCs at this time are shown on the right; data are mean values ± s.d. ($n=4$, $^{*}P<0.01$). (**F**) Bone pit formation assay. After differentiation of BMMs into osteoclasts on dentine slices, the slices were stained with haematoxylin and staining was quantitated using image analysis software. Representative images are shown in the upper panel (scale bar, 100 μm). Quantitative data are mean values ± s.d. ($n=3$, $^{*}P<0.01$). (**G**) Osteoclast differentiation from WT or *Rassf2*$^{-/-}$ BMMs co-cultured with WT or *Rassf2*$^{-/-}$ osteoblasts (Ob). TRAP-positive osteoclasts after co-culture for 9 days are shown in the left panels (scale bar, 100 μm), and the numbers of TRAP^{+} MNCs appear in the right panel; data are mean values ± s.d. ($n=4$, $^{*}P<0.01$). (**H**) After osteoblast differentiation in osteogenic media for the indicated times, RANKL, M-CSF, and OPG levels in culture media were measured by ELISA; the data are mean values ± s.d. ($n=3$, $^{*}P<0.01$). ND; not detected.

BMMs (Figure 3G). Notably, *Rassf2*$^{-/-}$ osteoblast precursors produced much less *Rankl* and *Csf1* mRNA, and secreted smaller levels of the encoded effectors (RANKL and M-CSF protein) into the culture medium during differentiation (Supplementary Figure S5; Figure 3C and H). This caused osteoclast formation from *Rassf2*$^{-/-}$ osteoblasts to fail. Together, the co-culture data strongly indicated that the osteoblast defects evident both *in vivo* and *in vitro* were a cell-autonomous consequence of *Rassf2* deficiency in the osteoblast progenitors. These observations further suggested that the osteoclast defect *in vivo* was due to the osteoblast defect, even though BMMs from *Rassf2*$^{-/-}$ mice showed intrinsic enhancement of the propensity towards osteoclast differentiation *in vitro*.

RASSF2 acts as an inhibitor of NF-κB signalling that is critical for differentiation of osteoclasts and osteoblasts

To determine the precise mechanism underlying the osteoclast stimulation and osteoblast inhibition associated with *Rassf2* deficiency *in vitro*, we examined the levels of intracellular signals required for osteoclast and osteoblast differentiation. Because NF-κB signalling is known to be important for both osteoclast and osteoblast differentiation, we first examined the status of such signalling. We found that *Rassf2* ablation resulted in marked enhancement of NF-κB signalling in *Rassf2*$^{-/-}$ BMMs, as reflected by phosphorylation of the NF-κB inhibitor IκBα; this is both an immediate and a delayed response to RANKL during osteoclast differentiation (Supplementary Figure S7A; Figure 4A). In addition, *Rassf2*$^{-/-}$ osteoblast precursors also showed enhanced NF-κB signalling, both before and during differentiation into osteoblasts, compared with WT cells (Supplementary Figure S7B; Figure 4B). Consistent with these results, global gene expression profiling revealed upregulation of positive regulators of NF-κB activity in *Rassf2*-deficient osteoblasts and osteoclasts both before and during differentiation, compared with WT cells (Figure 4C). We also observed that some of putative NF-κB target genes such as *Ppard*, *Htra3*, *Adrb2*, *Snrpd3*, *Gsdm2*, and *Tbc1d5* were downregulated in *Rassf2*-deficient osteoblasts but upregulated in *Rassf2*-deficient osteoclasts, both before and during differentiation (Supplementary Figure S8). These data suggested that a subset of known NF-κB target genes could be differentially regulated in the context of osteoblasts and osteoclasts. However, the roles played by these genes in osteoblast and osteoclast differentiation are not yet known. In this context, however, signalling by mitogen-activated protein kinases (MAPKs), including extracellular signal-regulated kinase, p38, and c-Jun NH_2-terminal kinase, did not significantly differ from that in *Rassf2*$^{-/-}$ BMMs (Figure 4A and D; Supplementary Figure S7A) or *Rassf2*$^{-/-}$ osteoblast precursors (Figure 4B and D; Supplementary Figure S7B), compared with WT cells. We finally examined whether restoration of RASSF2 might correct the defects in osteoclast and osteoblast differentiation associated with *Rassf2* ablation. To this end, we constructed a retroviral vector (pMX-Flag–RASSF2) encoding full-length human RASSF2. Reintroduction of RASSF2 into *Rassf2*$^{-/-}$ BMMs normalized the NF-κB signalling response to RANKL (Figure 4E) and restored differentiation of *Rassf2*$^{-/-}$ BMMs to the level of WT cells (Figure 4F). In addition, reintroduction of RASSF2 into *Rassf2*$^{-/-}$ osteoblast precursors attenuated the enhanced NF-κB signalling that was apparent before, and prompted, the differentiation response (Figure 4G). Also, such reintroduction rescued the reduced differentiation of *Rassf2*$^{-/-}$ osteoblast precursors to a level similar to that of the WT control (Figure 4H). Consistently, real-time PCR data revealed that, upon RASSF2 reintroduction, expression levels of osteoclastogenic (*Acp5* and *Nfatc1*) and osteoblastogenic gene markers (*Runx2*, *Sp7*, *Bglap1*, *Rankl*, and *Csf1*) were rescued to levels similar to those of WT cells (Supplementary Figure S9). Together, the genetic complementation data indicated that suppression of NF-κB signalling by RASSF2 indeed inhibited osteoclastogenesis, and stimulated osteoblastogenesis, *in vitro*.

RASSF2 associates with IKK and inhibits IKK activity

How does RASSF2 inhibit the NF-κB signalling cascade? We next attempted to identify NF-κB signalling targets for inhibition by RASSF2 using co-immunoprecipitation (co-IP). Importantly, we observed an association between RASSF2 and IκBα kinase α (IKKα) and β (IKKβ) (Figure 5A), both of which are overexpressed in 293T cells. We next sought to show an endogenous interaction between Rassf2 and IKK in osteoblast precursors. However, we found that no commercially available antibody against IKKα, IKKβ, or RASSF2 quantitatively precipitated the relevant protein. To overcome this technical difficulty, a retroviral vector encoding Flag-tagged RASSF2 was reintroduced into *Rassf2*$^{-/-}$ osteoblast precursors. We could then show that a small proportion of endogenous IKKα and IKKβ co-precipitated with Flag–RASSF2 from RASSF2-complemented cells (Figure 5B). Furthermore, an immune complex kinase assay revealed that coexpression of HA–RASSF2 inhibited the kinase activity of Flag–IKKα/β, as measured using a glutathione S-transferase (GST) fusion protein with IκBα as substrate (Figure 5C). This suggested that interaction of RASSF2 with IKK inhibited the activity of the kinase. To further confirm IKK inhibition by RASSF2, we performed an *in vitro* kinase assay using purified RASSF2, IKKβ, and IκBα proteins. Purified RASSF2 prevented IKKβ-mediated IκBα phosphorylation in a dose-dependent manner (Figure 5D). Consistently, the TNFα-induced activity of an NF-κB reporter gene was significantly inhibited by forced expression of RASSF2 (Figure 5E). Finally, subcellular fractionation and immunostaining assays revealed increased nuclear translocation of p65 in *Rassf2*$^{-/-}$ osteoblast precursors (Figure 5F and G), further demonstrating that NF-κB signalling was activated in such cells.

Finally, we attempted to clarify the genetic relationship between inhibition of IKK by RASSF2 and the effects of RASSF2 on osteoclast and osteoblast differentiation. We infected BMMs and osteoblast progenitors from *Rassf2*$^{-/-}$ mice with a retrovirus encoding a dominant-negative form of human IKKγ (IKK-DN); the encoded protein inhibits IKKα/β activity (Chang *et al*, 2009). Expression of IKK-DN in *Rassf2*$^{-/-}$ BMMs and osteoblast precursors attenuated the enhancement of NF-κB activation that is apparent in such cells upon induction of differentiation (Figure 6A and C). Furthermore, expression of IKK-DN restored the abnormally enhanced osteoclastogenesis of *Rassf2*$^{-/-}$ BMMs (Figure 6B) and the repressed osteoblastogenesis of *Rassf2*$^{-/-}$ osteoblast precursors to levels similar to those of WT cells (Figure 6D). Additionally, real-time PCR showed that IKK-DN overexpression in *Rassf2*$^{-/-}$ BMMs and osteoblast precursors restored the expression of osteoclastogenic (*Acp5* and *Nfatc1*) and osteoblastogenic gene markers (*Sp7*, *Rankl*, and *Csf1*) to

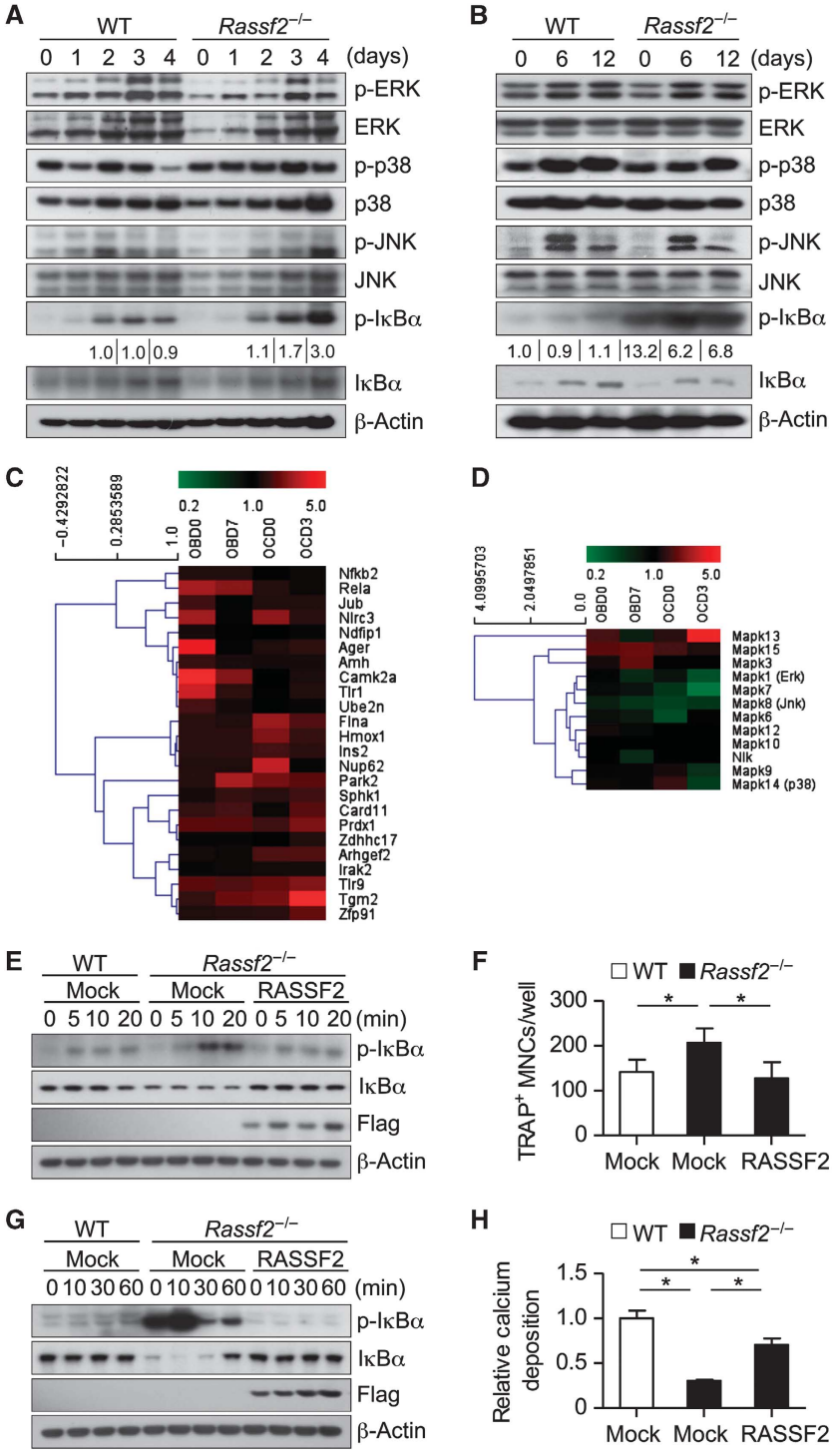

Figure 4 Loss of RASSF2 enhances NF-κB signalling associated with differentiation of osteoclasts and osteoblasts. (**A**) BMMs from WT and *Rassf2*$^{-/-}$ mice were cultured in the presence of RANKL and M-CSF for the indicated times to induce osteoclast differentiation, and cell lysates were next subjected to IB analysis using the indicated antibodies. (**B**) IB analysis of MAPK and NF-κB signalling molecules during WT and *Rassf2*$^{-/-}$ osteoblast differentiation in osteogenic medium containing bone morphogenetic protein 2, β-glycerophosphate, and ascorbic acid. The data in (**A**, **B**) are representative of those of three independent experiments. The band intensity of phosphorylated IκBα was normalized to the density of total IκBα, and the extent of phosphorylated IκBα in each test was next represented as a fold-induction relative to control (both for 2-day cultures undergoing osteoclast differentiation and for 0-day cultures undergoing osteoblast differentiation). (**C**, **D**) Gene expression profiling analyses of marker genes that are positive activators of NF-κB signalling (**C**) and MAP kinase activity (**D**). Expression of marker genes was analysed in *Rassf2*$^{-/-}$ osteoblast precursors or BMMs both before (day 0; OBD0 or OCD0) and during differentiation into osteoblasts or osteoclasts (day 7 or day 3; OBD7 or OCD3). Data are expressed relative to the values for WT cells. (**E**–**H**) BMMs (**E**, **F**) and osteoblast precursors (**G**, **H**) from WT or *Rassf2*$^{-/-}$ mice were infected with a retroviral vector encoding Flag-tagged RASSF2 or with the empty vector (Mock) and were next stimulated with RANKL (**E**, **F**) or osteogenic medium (**G**, **H**). Cell lysates prepared at the indicated times were subjected to IB analysis using antibodies to phosphorylated IκBα, IκBα, or Flag (**E**, **G**), and either the number of TRAP^{+} MNCs was determined after 4 days (**F**) or calcium deposition was measured after 12 days (**H**). Quantitative data are mean values ± s.d. ($n = 4$, $^{*}P < 0.01$).

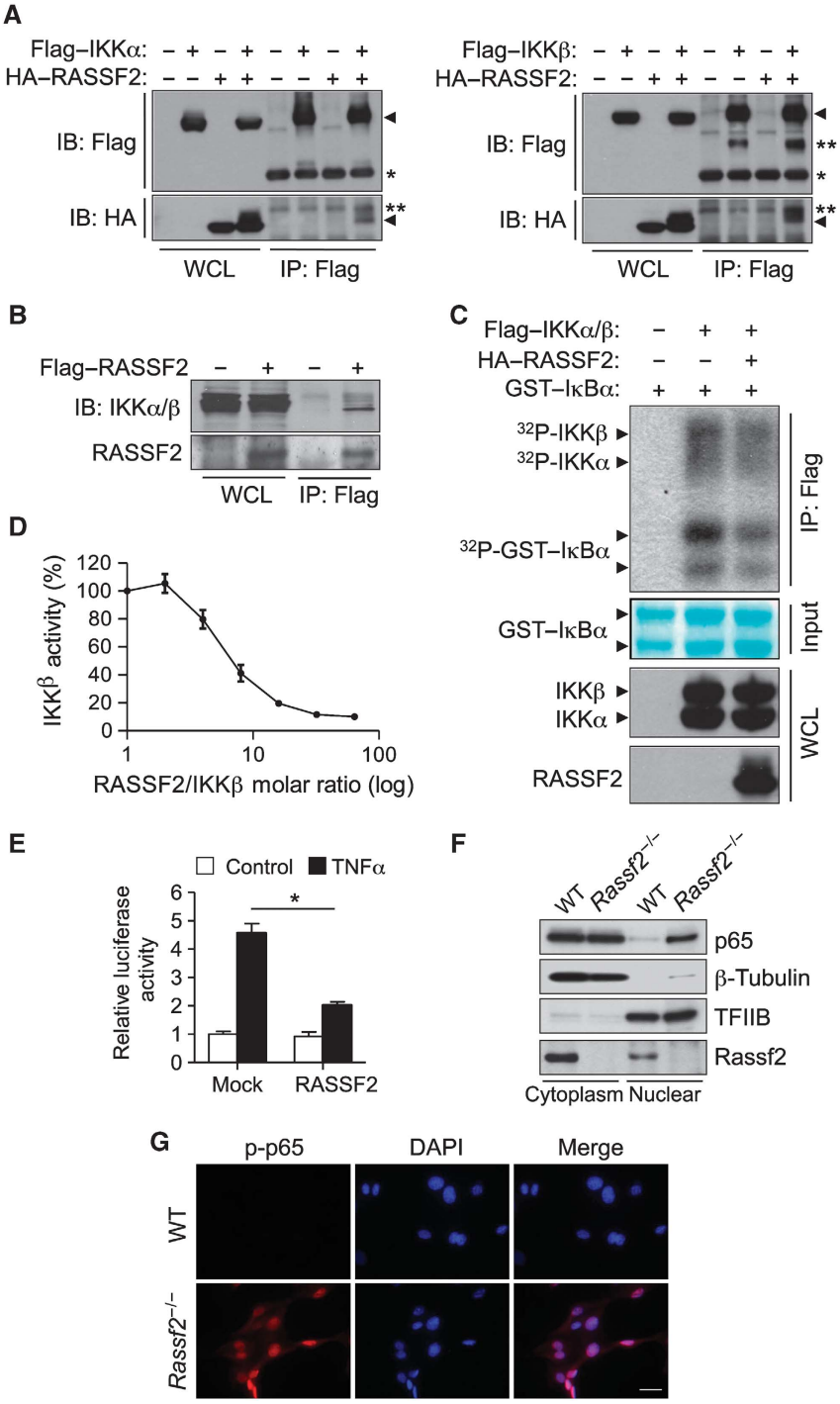

Figure 5 RASSF2 suppresses NF-κB signalling by inhibiting IKK activity. (**A**) 293T cells transfected with vectors encoding HA–RASSF2 and either Flag–IKKα (left panel) or Flag–IKKβ (right panel) were lysed and subjected to IP using an antibody directed against Flag. The resulting precipitates, and the corresponding whole-cell lysates (WCL), were subjected to IB analysis using the indicated antibodies; *Ig heavy chain; **non-specific band. (**B**) *Rassf2*$^{-/-}$ osteoblast precursors were infected with a retroviral vector encoding Flag-tagged RASSF2 or with the empty vector. Cell lysates were prepared and subjected to IP with antibody against Flag, and immunoblotted employing antibodies to RASSF2 or endogenous IKKα and β. (**C**) 293T cells expressing HA–RASSF2 and both Flag–IKKα and Flag–IKKβ were lysed and subjected to IP employing antibody against Flag, and the resulting precipitates were used in a kinase assay with [γ-^{32}P]ATP using GST–IκBα as a substrate (top panel). After autoradiography, the membrane was stained with Fast Green FCF to reveal substrate input (middle panel); and the cell lysates were subjected to IB analysis with antibody against Flag to detect IKKα and IKKβ, and with an antibody against HA to detect RASSF2 (bottom panels). (**D**) *In vitro* kinase assay data using different molar ratios of purified recombinant RASSF2 and IKKβ proteins. The IKKβ kinase activities (percentage values) were measured by estimating the extent of phosphorylation of GST–IκBα, and were plotted against the RASSF2 versus IKKβ molar ratio (logarithmic scale). (**E**) C2C12 cells transiently transfected with an NF-κB reporter construct and either a vector encoding HA–RASSF2 or the empty vector (Mock) were incubated in the absence (Control) or presence of TNFα (20 ng/ml), lysed, and next assayed for luciferase activity; the data are mean values ± s.d. ($n = 3$, $^*P < 0.01$). (**F**) Nuclear/cytoplasmic fractionation. Subcellular fractionation was performed on WT or *Rassf2*$^{-/-}$ osteoblast precursors. Nuclear and cytoplasmic lysates were subjected to IB analysis with antibodies against p65 and Rassf2. β-Tubulin and TFIIB, respectively, were used as controls in the analysis of cytoplasmic and nuclear fractions. (**G**) Immunostaining analysis. WT or *Rassf2*$^{-/-}$ osteoblast precursors were subjected to immunostaining using an antibody against phosphorylated p65. Note that mutant cells showed highly increased nuclear translocation of activated p65.

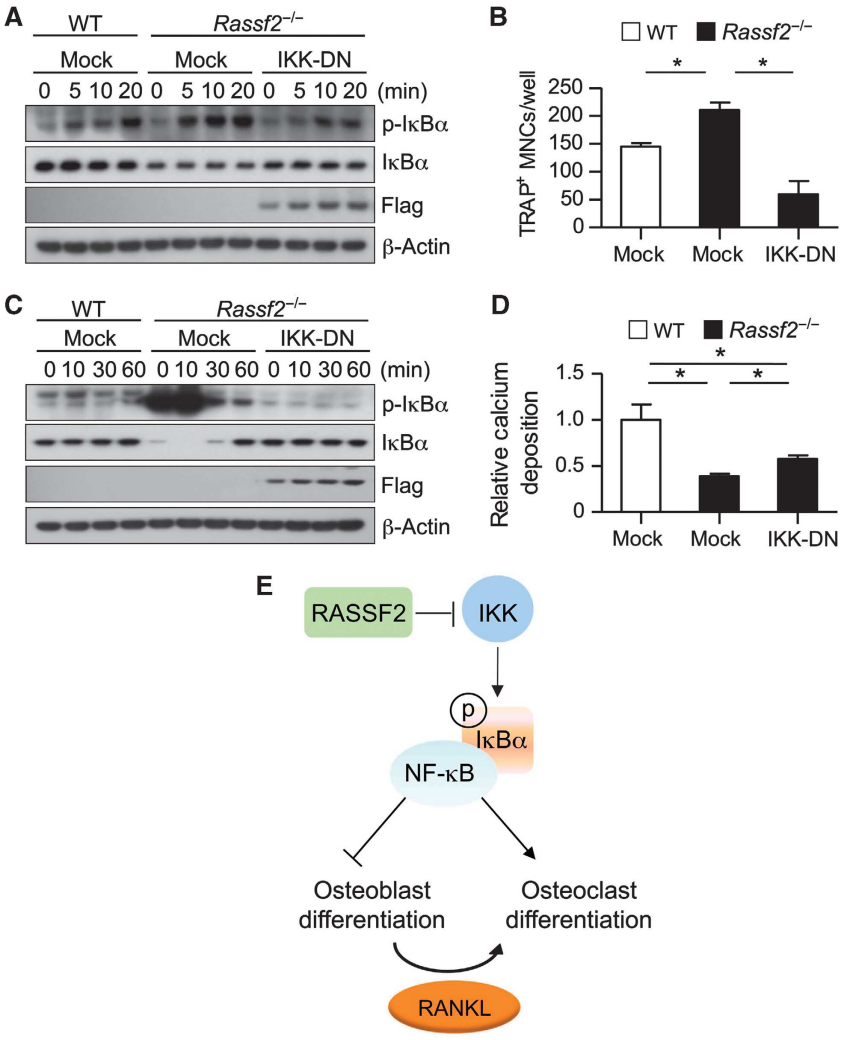

Figure 6 Inhibition of IKK activity restores the deregulated differentiation of *Rassf2*-deficient osteoclasts and osteoblasts. (**A**–**D**) BMMs (**A**, **B**) and osteoblast precursors (**C**, **D**) from WT or *Rassf2*$^{-/-}$ mice were infected with a retroviral vector encoding Flag-tagged IKK-DN or with the empty vector, and were next stimulated with RANKL (**A**, **B**) or osteogenic medium (**C**, **D**). Cell lysates prepared at the indicated times were subjected to IB analysis with the indicated antibodies (**A**, **C**), and either the number of TRAP^{+} MNCs was determined after 4 days (**B**) or calcium deposition was measured after 12 days (**D**). Quantitative data are mean values ± s.d. ($n = 4$, $^{*}P < 0.01$). (**E**) Model for RASSF2-mediated inhibition of NF-κB signalling during osteoclast and osteoblast differentiation.

levels similar to those of WT cells (Supplementary Figure S10). Together, the data show that hyperactivation of NF-κB signalling induced by loss of *Rassf2* can be normalized by expression of IKK-DN during both osteoblast and osteoclast differentiation. Our work thus suggests that RASSF2 suppresses NF-κB signalling by inhibiting IKK activity, consequently attenuating osteoclastogenesis and stimulating osteoblastogenesis (Figure 6E).

Discussion

Osteoporotic bone diseases including postmenopausal osteoporosis, arthritis, periodontitis, bone metastasis of cancer, and Paget's disease are mostly attributable to excessive bone destruction by osteoclasts relative to bone formation by osteoblasts (Boyle *et al*, 2003; Novack and Teitelbaum, 2008). An optimal anti-osteoporotic agent would thus both inhibit the activation of bone-degrading osteoclasts and promote the actions of bone-forming osteoblasts. NF-κB signaling is known to activate osteoclast differentiation and to suppress osteoblast differentiation (Jimi *et al*, 2004; Chang *et al*, 2009). A cell-permeable selective inhibitor of NF-κB signalling was recently shown to block the inflammatory bone loss that results from enhanced osteoclast formation (Jimi *et al*, 2004). Osteoblast-specific inhibition of IKK–NF-κB signalling has been shown to prevent the bone loss associated with oestrogen deficiency by maintaining osteoblastic bone formation (Chang *et al*, 2009). Recent studies using an *in vitro* reporter assay have shown that RASSF1A, RASSF2, RASSF6, and RASSF8 all inhibit the transactivation activity of NF-κB (Allen *et al*, 2007; Imai *et al*, 2008; Del Re *et al*, 2010; Lock *et al*, 2010). However, neither the molecular mechanism of action nor the role played by RASSF-mediated NF-κB regulation during bone development has been determined.

Our present study provides novel insights into the role of RASSF2 in mammalian bone remodelling. Our conclusions are supported by the following observations: (i) *Rassf2*-null mice exhibit reductions in the numbers of osteoblasts

and osteoclasts and the rate of bone formation (Figure 2); (ii) *in vitro* differentiation studies reveal that cells from *Rassf2*$^{-/-}$ mice show reduced osteoblast differentiation and enhanced osteoclast differentiation (Figure 3); (iii) *Rassf2*$^{-/-}$ cells demonstrate reduced expression levels of osteoblast differentiation markers and increased expression levels of osteoclast differentiation markers (Figure 3; Supplementary Figures S5 and S6); and (iv) co-culture studies show that WT osteoblasts support enhanced osteoclastic differentiation of *Rassf2*$^{-/-}$ BMMs compared with that of WT BMMs, whereas *Rassf2*$^{-/-}$ osteoblasts do not induce osteoclast formation from either WT or *Rassf2*$^{-/-}$ BMMs (Figure 3). Collectively, we conclude that a reduction in the number of osteoblasts expressing osteoclastogenic factors eventually impairs osteoclast formation in *Rassf2*-null mice. At the molecular level, *Rassf2* ablation resulted in enhanced phosphorylation of the NF-κB inhibitor IκBα during both osteoclast and osteoblast differentiation, indicating hyperactivation of NF-κB signalling (Figure 4). Our biochemical studies further show that purified RASSF2 inhibits the activity of IKK. Finally, overexpression of a dominant-negative form of IKK in *Rassf2*$^{-/-}$ osteoclast or osteoblast precursors inhibits NF-κB hyperactivation and normalizes both osteoclast and osteoblast differentiation (Figure 6), revealing the genetic interaction between RASSF2 and IKK in such cell contexts. Based on these results, we suggest that RASSF2 suppresses NF-κB signalling through an inhibitory association with IKK, and that RASSF2 consequently attenuates osteoclastogenesis and stimulates osteoblastogenesis.

The Hippo pathway has been implicated in both developmental processes and tumourigenesis, and in the control of the size of organs such as the liver (Camargo *et al*, 2007; Dong *et al*, 2007; Lee *et al*, 2008, 2010; Zhou *et al*, 2009; Lian *et al*, 2010; Lu *et al*, 2010; Zhang *et al*, 2010; Song *et al*, 2010a). In addition, *Nf2*/Merlin, an upstream component of the Hippo signalling pathway, maintains the bone microenvironment by regulating osteoblast numbers and the level of the HSC pool (Larsson *et al*, 2008). We and others have recently shown that MST is a major binding partner of RASSF2 and that the stability of both proteins is regulated in a reciprocal manner (Cooper *et al*, 2009; Song *et al*, 2010b). *Mst1*-deficient mice exhibit reduced levels of naive T cells in all of the peripheral blood, the spleen, and LNs, and lack marginal zone B cells in the spleen (Zhou *et al*, 2008; Choi *et al*, 2009). Similarly, *Nore1b*-null mice have reduced lymphocyte numbers in peripheral lymphoid organs and fewer hypoplastic B-cell follicles in the Peyer's patches and spleen (Katagiri *et al*, 2004). However, despite the fact that expression of the genes is ubiquitous, neither *Mst1* nor *Nore1b* deficiency caused significant growth retardation; abnormalities were present only in lymphoid organs. Importantly, we found that depletion of *Rassf2* in mice resulted in systemic lymphopenia accompanying severe bone defects. The reduction in lymphocyte numbers in *Rassf2*$^{-/-}$ mice may not be attributable to cell-autonomous defects affecting the repopulation capacity of *Rassf2*$^{-/-}$ HSCs (Figure 1E). Although *Rassf2*$^{-/-}$ BMMs manifested intrinsic differentiation enhancement (Figure 3E), our findings of reduced levels of HSCs in *Rassf2*$^{-/-}$ mice (Figure 1D) and impaired differentiation of *Rassf2*$^{-/-}$ BMMs towards *Rassf2*$^{-/-}$ osteoblast precursors (Figure 3G) further suggest that impaired bone remodelling in *Rassf2*$^{-/-}$ mice is likely attributable to reduced bone turnover caused by defects in both osteoclast and osteoblast formation. However, we cannot currently exclude the possibility that *Rassf2* deficiency causes intrinsic defects in lymphoid organ development, immune cell differentiation, or maintenance of HSCs or MSCs. Therefore, in the light of the fact that crosstalk occurs between the immune and skeletal system of *Rassf2*$^{-/-}$ mice, tissue-specific depletion of *Rassf2* will be required to identify, in more detail, the roles played by RASSF2 during haematopoietic development and bone remodelling.

To date, the Hippo pathway in mammals has been extensively studied with respect only to epithelial developments and to control of organ size. No obvious bone defects have yet been reported in *Mst1*, *Rassf1*, *Lats1*, or *Nore1b*-deficient mice. Importantly, we also found that expression of both Hippo components and Rassf2 gradually increased during differentiation of WT osteoclasts and osteoblasts (Supplementary Figure S11). Moreover, Hippo component expression, such as that of Mst1, Mst2, or Lats1, was apparently reduced in *Rassf2*-deficient osteoclasts and osteoblasts (Supplementary Figure S11). Therefore, it is possible that Hippo components play roles in bone development. In addition, RASSF2, among the RASSF protein family, may serve as a specific integrator of the Hippo signalling network during bone development. Thus, it will be necessary to determine whether bone-specific deletion of Hippo components such as Mst1/2 and Lats1/2 also result in deregulated bone cell differentiation.

Materials and methods

Generation of Rassf2 knockout mice

The *Rassf2* genomic locus encompassing exons 2–9 was isolated from a 129/SvJ mouse BAC (bacterial artificial chromosome) library. For construction of the targeting vector, a 3858-bp right-arm fragment obtained by PCR was subcloned into the *Bam*HI site of the PGK-puro targeting vector, after which a 5237-bp left-arm fragment, also obtained by PCR, was subcloned into the *Eco*RI site of the same vector. The diphtheria toxin A gene (DT-A) was next inserted into the *Not*I site at the 3′ end of the right arm, to permit negative selection. A genomic region (3.99 kb) spanning exons 4 and 5 of *Rassf2* was thus replaced with a 1.5-kb fragment containing the puromycin-resistance gene (Puro), a positive selection marker. Generation of *Rassf2* knockout mice was accomplished using standard methods permitting homologous recombination in embryonic stem cells, followed by blastocyst injection. The correct recombination event was confirmed by Southern blotting, genotyping of genomic DNA, and RT–PCR detecting *Rassf2* mRNA in mouse embryonic fibroblasts. The primers for mouse genotyping were 5′-AAC AAA CTA GAA CAA TCC TGT CGT C-3′ (forward) for the WT and mutant alleles of *Rassf2*; and 5′-CAA GAC CCT GTT TCT TTA AAA CTG A-3′ (reverse) for the WT allele and 5′-GCA CGA GAC TAG TGA GAC GTG CTA C-3′ (reverse) for the mutant allele. Primers for RT–PCR were 5′-TGT GGA GGG GTT ACT GAA CA-3′ (forward) and 5′-AGC CAT AGG CTG GTG TGA AC-3′ (reverse); PCR yielded a product of 413 bp from *Rassf2*. *Rassf2*$^{-/-}$ mice were backcrossed into C57BL/6 animals for more than seven generations. Animal care and experimentation complied with procedures approved by the KAIST Animal Care and Use Committee (KACUC).

Retrovirus preparation and infection

For preparation of retroviral particles, 293T cells were transfected with pMX vectors encoding Flag-tagged human RASSF2 or Flag-tagged human IKK-DN (or with empty vector) employing polyethylenimine (Polysciences). After 3 days, the medium containing retroviruses was harvested and passed through a syringe filter 0.2 μm in pore diameter. BMMs or primary osteoblast cells were infected with retroviruses for 6 h employing polybrene (8 μg/ml) in the presence or absence of M-CSF (120 ng/ml). After washing with

fresh medium, BMMs or osteoblast cells were cultured for 2 days in the presence of puromycin (2 μg/ml) with or without M-CSF (120 ng/ml). Puromycin-resistant BMMs or osteoblast cells were next studied.

RT–PCR and protein analyses

Isolation of total RNA, and cDNA synthesis, were performed following the protocols of the manufacturer of the kit (Intron). The sequences of the various PCR primers are available on request. Antibodies used in IB analysis included those against Flag (Sigma); HA (Covance); and Fra-1, Runx2, c-Src, c-Fos, NFATc1, phosphorylated IκBα, IκBα, p65, and β-actin (Santa Cruz Biotechnology). Antibody against RASSF2 was generated as previously described (Song *et al*, 2010b). All other antibodies were obtained from Cell Signaling. Co-IP and immune complex kinase assays were performed as described previously (Song *et al*, 2010b). Purified histidine-tagged RASSF2 protein, GST–IKKβ (Cell Signaling), and GST–IκBα, were used in the *in vitro* kinase assay. The kinase activity of IKKβ was measured by incubating 15 nM of GST–IKKβ, 300 nM of GST–IκBα (as a substrate), and the indicated molar ratios of RASSF2, in kinase buffer (25 mM Tris–HCl (pH 7.5), 10 mM $MgCl_2$, 0.1 mM Na_3VO_4, 5 mM β-glycerophosphate, 2 mM dithiothreitol, and 3 μCi (γ-^{32}P) ATP) for 30 min at 30°C. The levels of phosphorylated GST–IκBα were measured by autoradiography. The NF-κB reporter assay was performed using the firefly luciferase reporter plasmid pNF-κB-Luc (Stratagene) and the *Renilla* luciferase control plasmid pRL-TK (Promega); the activity of firefly luciferase was determined using the Dual-Luciferase reporter assay system (Promega). Subcellular fractionation was performed using NE-PER Nuclear and Cytoplasmic Extraction Reagents, as per the protocols of the manufacturer (Thermo Scientific). Immunostaining employed a phospho-p65 antibody (Abcam) and was performed as previously described (Lee *et al*, 2008).

Microcomputed tomography, histological analysis, measurement of mineral deposition rate, and assay of osteoclast-regulating and bone resorption markers

The proximal tibia (sections 18 μm thick) was scanned in three dimensions using a high-resolution microcomputed tomography scanner (Skyscan 1076 Micro-CT System). For analysis of bone histology, serial 5 μm-thick sagittal sections were prepared with the use of a microtome and were stained either with H&E to detect osteoblasts or with TRAP to visualize osteoclasts. Counterstaining employed methylene blue. For analysis of MAR, mice were intraperitoneally injected with calcein (15 mg/kg of body weight; Sigma) on postnatal days 13 and day 23 and were sacrificed 3 days after the final injection. Bones were sectioned and calcein double-labelled bone surfaces were photographed to measure the rate of mineral apposition. For measurement of M-CSF, RANKL, and osteoprotegerin (OPG) (all of which regulate osteoclast formation); and type 1 collagen CTX (a known bone resorption marker); sera and urine were collected from 3-week-old WT and *Rassf2*$^{-/-}$ mice. Osteoclast-regulating factors (RANKL, M-CSF, and OPG) in sera, and CTX in sera and urine, were measured using commercial immunoassay kits from R&D Systems and IDS Ltd., respectively.

Osteoclast and osteoblast differentiation

For analysis of osteoclast differentiation, BMMs (osteoclast precursors) were obtained from cultures of BM cells isolated from the tibia and femur of 3-week-old male mice, as described (Kim *et al*, 2009). BMMs were cultured for 4 days in α-minimum essential medium (α-MEM) supplemented with M-CSF (30 ng/ml) and RANKL (100 ng/ml). The cells were next fixed and stained for TRAP employing a leukocyte acid phosphatase staining kit (Sigma). TRAP-positive cells containing $\geqslant$10 nuclei, and an actin ring, were counted with the aid of a light microscope. For analysis of bone pit formation, BMMs (5×10^3 cells/well in 96-well plates) were seeded onto dentine slices (IDS Ltd.) and were allowed to differentiate into osteoclasts in the presence of M-CSF and RANKL for 6 days, with a change of medium after 2 days. After all slices were subjected to ultrasonication to remove adherent cells, and stained with haematoxylin, pit areas were photographed under a light microscope and analysed using Image-Pro Plus version 6.0 software (MediaCybernetics). For analysis of osteoblast differentiation, primary osteoblast cells were prepared from the calvarium of newborn mice by five sequential digestions with dispase II and collagenase type IA. Primary osteoblast cells (1×10^4 cells/well in 48-well plates) were cultured in osteogenic medium (α-MEM supplemented with 10% FBS, bone morphogenetic protein 2 (100 ng/ml; R&D Systems), 10 mM β-glycerophosphate, and ascorbic acid (100 μg/ml)) for 12 days. Mineralized nodule formation was determined on days 6 and 12 by staining with alizarin red S solution (2%, pH 4.2). For quantitation of calcium deposition, cells were washed with distilled water, the dye was eluted with 10% cetylpyridinium chloride, and absorbance at 595 nm was measured with the use of a microplate reader (Bio-Rad). In the co-culture experiments, BMMs (1×10^5 cells/well in 48-well plates) were cultured with calvarial osteoblast cells (1×10^4 cells/well) in the presence of 20 nM 1α,25-dyhydroxy vitamin D_3 and 1 μM prostaglandin E_2 to induce expression of osteoclastogenic M-CSF and RANKL and to permit osteoclast differentiation over 9 days.

Flow cytometric analysis

Thymus and spleen tissue digests were passed through a Cell Strainer 40 μm in pore diameter (BD Falcon) and cells in the filtrate were isolated by centrifugation employing lymphocyte separation medium (Mediatech Cellgro). For isolation of peripheral blood leukocytes, blood from the tail vein was suspended with a solution containing 0.15 M NH_4Cl, 10 mM $KHCO_3$, and 0.1 mM EDTA (disodium salt) at pH 7.2. Isolated cells were stained with fluorescein isothiocyanate (FITC)-conjugated antibody to CD4 and phycoerythrin (PE)-conjugated antibody to CD8α for analysis of T lymphocytes, and with FITC-conjugated antibody to B220 for analysis of B lymphocytes. To detect LSK and MP cells, BM cells were prepared by flushing of the femur and tibia with Dulbecco's modified Eagle's medium supplemented with 2% (v/v) FBS and antibiotics followed by centrifugation using lymphocyte separation medium. Isolated BM cells were stained with biotin-conjugated antibodies to lineage markers (CD4, CD8α, B220, Gr-1, CD11b, and Ter119); FITC-conjugated antibody to CD34; PE-conjugated antibody to Flk2; PE-Cy7-conjugated antibody to Sca1; and allophycocyanin (APC)-conjugated antibody to c-Kit. APC-Cy7-conjugated streptavidin was next used to detect lineage markers. Stained cells were analysed with a FACSCalibur or LSRII flow cytometer (BD Biosciences).

BM transplantation

BM cells were harvested from the femur and tibia of 3-week-old WT or *Rassf2*$^{-/-}$ mice, as described above. For competitive transplantation, CD45.1$^+$ competitor BM cells (1×10^6) from WT C57BL/6J mice and CD45.2$^+$ donor BM cells (2×10^6) from *Rassf2*$^{+/+}$ or *Rassf2*$^{-/-}$ mice were mixed in a 2:1 ratio and next injected into the tail vein of lethally irradiated (10 Gy) C57BL/6J recipient mice. CD45.2$^+$ donor cells in peripheral blood of recipient mice were quantitated at the indicated times thereafter by staining with PE-conjugated antibody to CD45.1 and FITC-conjugated antibody to CD45.2, followed by flow cytometry.

Global gene expression profiling analyses

Global gene expression analyses were performed by eBiogen Inc., using the Agilent Mouse whole-genome 44K platform. Data were analysed using Agilent's GeneSpring GX software. Heatmap representation was achieved using the TIGR Multiexperiment Viewer program MeV version 4.6. For analysis of marker genes related to positive regulators of NF-κB activity, significantly upregulated genes were selected by hierarchical clustering analysis using average linkage and Euclidean distance values and assigned to the biological pathways GO 0042345, GO 0042346, GO 0051092, GO 0043123, GO 0033257, GO 0007250, GO 0008588, or GO 0043122.

Statistical analysis

Data are presented as mean values ± s.e.m. or ± s.d., as indicated, and were analysed using Student's two-tailed *t*-test. A *P*-value <0.05 was considered to be statistically significant.

Supplementary data

Supplementary data are available at *The EMBO Journal* Online (http://www.embojournal.org).

Acknowledgements

We thank NS Kim for comments on the manuscript. This study was supported by grants from the National Creative Research Initiatives Center Program (no. 2010-0018277) and the WCU Program (no. R31-2008-000-10071-0, to D-SL), and by grants from the National Research Foundation of Korea funded by the Korean Government (nos. 2011-0006178 and 2010-0012161, to DJ).

Author contributions: HS, HK, DJ, and D-SL designed the project; HS and HK performed most of the experiments with help from KL, D-HL, T-SK, JYS, DL, DC, and CP; C-YK, H-SK, and H-IS conducted bone histology; JC and HP assisted with flow cytometric analysis and provided reagents for some experiments; DJ and D-SL were involved in all aspects of data analysis and preparation of the manuscript.

Conflict of interest

The authors declare that they have no conflict of interest.

References

Allen NP, Donninger H, Vos MD, Eckfeld K, Hesson L, Gordon L, Birrer MJ, Latif F, Clark GJ (2007) RASSF6 is a novel member of the RASSF family of tumor suppressors. *Oncogene* **26:** 6203–6211

Arai F, Hirao A, Ohmura M, Sato H, Matsuoka S, Takubo K, Ito K, Koh GY, Suda T (2004) Tie2/angiopoietin-1 signaling regulates hematopoietic stem cell quiescence in the bone marrow niche. *Cell* **118:** 149–161

Boyle WJ, Simonet WS, Lacey DL (2003) Osteoclast differentiation and activation. *Nature* **423:** 337–342

Calvi LM, Adams GB, Weibrecht KW, Weber JM, Olson DP, Knight MC, Martin RP, Schipani E, Divieti P, Bringhurst FR, Milner LA, Kronenberg HM, Scadden DT (2003) Osteoblastic cells regulate the haematopoietic stem cell niche. *Nature* **425:** 841–846

Camargo FD, Gokhale S, Johnnidis JB, Fu D, Bell GW, Jaenisch R, Brummelkamp TR (2007) YAP1 increases organ size and expands undifferentiated progenitor cells. *Curr Biol* **17:** 2054–2060

Chang J, Wang Z, Tang E, Fan Z, McCauley L, Franceschi R, Guan K, Krebsbach PH, Wang CY (2009) Inhibition of osteoblastic bone formation by nuclear factor-kappaB. *Nat Med* **15:** 682–689

Choi J, Oh S, Lee D, Oh HJ, Park JY, Lee SB, Lim DS (2009) Mst1-FoxO signaling protects naive T lymphocytes from cellular oxidative stress in mice. *PLoS One* **4:** e8011

Cooper WN, Dickinson RE, Dallol A, Grigorieva EV, Pavlova TV, Hesson LB, Bieche I, Broggini M, Maher ER, Zabarovsky ER, Clark GJ, Latif F (2008) Epigenetic regulation of the ras effector/tumour suppressor RASSF2 in breast and lung cancer. *Oncogene* **27:** 1805–1811

Cooper WN, Hesson LB, Matallanas D, Dallol A, von Kriegsheim A, Ward R, Kolch W, Latif F (2009) RASSF2 associates with and stabilizes the proapoptotic kinase MST2. *Oncogene* **28:** 2988–2998

Del Re DP, Matsuda T, Zhai P, Gao S, Clark GJ, Van Der Weyden L, Sadoshima J (2010) Proapoptotic Rassf1A/Mst1 signaling in cardiac fibroblasts is protective against pressure overload in mice. *J Clin Invest* **120:** 3555–3567

Dong J, Feldmann G, Huang J, Wu S, Zhang N, Comerford SA, Gayyed MF, Anders RA, Maitra A, Pan D (2007) Elucidation of a universal size-control mechanism in Drosophila and mammals. *Cell* **130:** 1120–1133

Imai T, Toyota M, Suzuki H, Akino K, Ogi K, Sogabe Y, Kashima L, Maruyama R, Nojima M, Mita H, Sasaki Y, Itoh F, Imai K, Shinomura Y, Hiratsuka H, Tokino T (2008) Epigenetic inactivation of RASSF2 in oral squamous cell carcinoma. *Cancer Sci* **99:** 958–966

Jimi E, Aoki K, Saito H, D'Acquisto F, May MJ, Nakamura I, Sudo T, Kojima T, Okamoto F, Fukushima H, Okabe K, Ohya K, Ghosh S (2004) Selective inhibition of NF-kappa B blocks osteoclastogenesis and prevents inflammatory bone destruction *in vivo*. *Nat Med* **10:** 617–624

Katagiri K, Ohnishi N, Kabashima K, Iyoda T, Takeda N, Shinkai Y, Inaba K, Kinashi T (2004) Crucial functions of the Rap1 effector molecule RAPL in lymphocyte and dendritic cell trafficking. *Nat Immunol* **5:** 1045–1051

Kim H, Choi HK, Shin JH, Kim KH, Huh JY, Lee SA, Ko CY, Kim HS, Shin HI, Lee HJ, Jeong D, Kim N, Choi Y, Lee SY (2009) Selective inhibition of RANK blocks osteoclast maturation and function and prevents bone loss in mice. *J Clin Invest* **119:** 813–825

Larsson J, Ohishi M, Garrison B, Aspling M, Janzen V, Adams GB, Curto M, McClatchey AI, Schipani E, Scadden DT (2008) Nf2/merlin regulates hematopoietic stem cell behavior by altering microenvironmental architecture. *Cell Stem Cell* **3:** 221–227

Lee JH, Kim TS, Yang TH, Koo BK, Oh SP, Lee KP, Oh HJ, Lee SH, Kong YY, Kim JM, Lim DS (2008) A crucial role of WW45 in developing epithelial tissues in the mouse. *EMBO J* **27:** 1231–1242

Lee KP, Lee JH, Kim TS, Kim TH, Park HD, Byun JS, Kim MC, Jeong WI, Calvisi DF, Kim JM, Lim DS (2010) The Hippo-Salvador pathway restrains hepatic oval cell proliferation, liver size, and liver tumorigenesis. *Proc Natl Acad Sci USA* **107:** 8248–8253

Lian I, Kim J, Okazawa H, Zhao J, Zhao B, Yu J, Chinnaiyan A, Israel MA, Goldstein LS, Abujarour R, Ding S, Guan KL (2010) The role of YAP transcription coactivator in regulating stem cell self-renewal and differentiation. *Genes Dev* **24:** 1106–1118

Lock FE, Underhill-Day N, Dunwell T, Matallanas D, Cooper W, Hesson L, Recino A, Ward A, Pavlova T, Zabarovsky E, Grant MM, Maher ER, Chalmers AD, Kolch W, Latif F (2010) The RASSF8 candidate tumor suppressor inhibits cell growth and regulates the Wnt and NF-kappaB signaling pathways. *Oncogene* **29:** 4307–4316

Lu L, Li Y, Kim SM, Bossuyt W, Liu P, Qiu Q, Wang Y, Halder G, Finegold MJ, Lee JS, Johnson RL (2010) Hippo signaling is a potent *in vivo* growth and tumor suppressor pathway in the mammalian liver. *Proc Natl Acad Sci USA* **107:** 1437–1442

Maruyama R, Akino K, Toyota M, Suzuki H, Imai T, Ohe-Toyota M, Yamamoto E, Nojima M, Fujikane T, Sasaki Y, Yamashita T, Watanabe Y, Hiratsuka H, Hirata K, Itoh F, Imai K, Shinomura Y, Tokino T (2008) Cytoplasmic RASSF2A is a proapoptotic mediator whose expression is epigenetically silenced in gastric cancer. *Carcinogenesis* **29:** 1312–1318

Matsuo K, Irie N (2008) Osteoclast-osteoblast communication. *Arch Biochem Biophys* **473:** 201–209

McPherson JP, Tamblyn L, Elia A, Migon E, Shehabeldin A, Matysiak-Zablocki E, Lemmers B, Salmena L, Hakem A, Fish J, Kassam F, Squire J, Bruneau BG, Hande MP, Hakem R (2004) Lats2/Kpm is required for embryonic development, proliferation control and genomic integrity. *EMBO J* **23:** 3677–3688

Morin-Kensicki EM, Boone BN, Howell M, Stonebraker JR, Teed J, Alb JG, Magnuson TR, O'Neal W, Milgram SL (2006) Defects in yolk sac vasculogenesis, chorioallantoic fusion, and embryonic axis elongation in mice with targeted disruption of Yap65. *Mol Cell Biol* **26:** 77–87

Nilsson SK, Johnston HM, Whitty GA, Williams B, Webb RJ, Denhardt DT, Bertoncello I, Bendall LJ, Simmons PJ, Haylock DN (2005) Osteopontin, a key component of the hematopoietic stem cell niche and regulator of primitive hematopoietic progenitor cells. *Blood* **106:** 1232–1239

Novack DV, Teitelbaum SL (2008) The osteoclast: friend or foe? *Annu Rev Pathol* **3:** 457–484

Oh S, Lee D, Kim T, Kim TS, Oh HJ, Hwang CY, Kong YY, Kwon KS, Lim DS (2009) Crucial role for Mst1 and Mst2 kinases in early embryonic development of the mouse. *Mol Cell Biol* **29:** 6309–6320

Pan D (2010) The Hippo signaling pathway in development and cancer. *Dev Cell* **19:** 491–505

Park J, Kang SI, Lee SY, Zhang XF, Kim MS, Beers LF, Lim DS, Avruch J, Kim HS, Lee SB (2010) Tumor suppressor ras association domain family 5 (RASSF5/NORE1) mediates death receptor ligand-induced apoptosis. *J Biol Chem* **285:** 35029–35038

Ren J, He W, Zhang R, Li Z, Cao W, Yao J, Zhu F, Zhang T, Wu G (2009) RASSF2A promoter methylation in hepatitis B virus-related hepatocellular carcinogenesis and its correlation with elevated serum alpha-fetoprotein level. *J Huazhong Univ Sci Technolog Med Sci* **29:** 309–312

Song H, Mak KK, Topol L, Yun K, Hu J, Garrett L, Chen Y, Park O, Chang J, Simpson RM, Wang CY, Gao B, Jiang J, Yang Y (2010a) Mammalian Mst1 and Mst2 kinases play essential roles in organ size control and tumor suppression. *Proc Natl Acad Sci USA* **107:** 1431–1436

Song H, Oh S, Oh HJ, Lim DS (2010b) Role of the tumor suppressor RASSF2 in regulation of MST1 kinase activity. *Biochem Biophys Res Commun* **391:** 969–973

Stier S, Ko Y, Forkert R, Lutz C, Neuhaus T, Grunewald E, Cheng T, Dombkowski D, Calvi LM, Rittling SR, Scadden DT (2005) Osteopontin is a hematopoietic stem cell niche component that negatively regulates stem cell pool size. *J Exp Med* **201:** 1781–1791

Sudol M, Harvey KF (2010) Modularity in the Hippo signaling pathway. *Trends Biochem Sci* **35:** 627–633

Takayanagi H (2007) Osteoimmunology: shared mechanisms and crosstalk between the immune and bone systems. *Nat Rev Immunol* **7:** 292–304

Tommasi S, Dammann R, Zhang Z, Wang Y, Liu L, Tsark WM, Wilczynski SP, Li J, You M, Pfeifer GP (2005) Tumor susceptibility of Rassf1a knockout mice. *Cancer Res* **65:** 92–98

van der Weyden L, Tachibana KK, Gonzalez MA, Adams DJ, Ng BL, Petty R, Venkitaraman AR, Arends MJ, Bradley A (2005) The RASSF1A isoform of RASSF1 promotes microtubule stability and suppresses tumorigenesis. *Mol Cell Biol* **25:** 8356–8367

Visnjic D, Kalajzic Z, Rowe DW, Katavic V, Lorenzo J, Aguila HL (2004) Hematopoiesis is severely altered in mice with an induced osteoblast deficiency. *Blood* **103:** 3258–3264

Vos MD, Ellis CA, Elam C, Ulku AS, Taylor BJ, Clark GJ (2003) RASSF2 is a novel K-Ras-specific effector and potential tumor suppressor. *J Biol Chem* **278:** 28045–28051

Walsh MC, Kim N, Kadono Y, Rho J, Lee SY, Lorenzo J, Choi Y (2006) Osteoimmunology: interplay between the immune system and bone metabolism. *Annu Rev Immunol* **24:** 33–63

Zhang J, Niu C, Ye L, Huang H, He X, Tong WG, Ross J, Haug J, Johnson T, Feng JQ, Harris S, Wiedemann LM, Mishina Y, Li L (2003) Identification of the haematopoietic stem cell niche and control of the niche size. *Nature* **425:** 836–841

Zhang N, Bai H, David KK, Dong J, Zheng Y, Cai J, Giovannini M, Liu P, Anders RA, Pan D (2010) The Merlin/NF2 tumor suppressor functions through the YAP oncoprotein to regulate tissue homeostasis in mammals. *Dev Cell* **19:** 27–38

Zhao B, Lei QY, Guan KL (2008) The Hippo-YAP pathway: new connections between regulation of organ size and cancer. *Curr Opin Cell Biol* **20:** 638–646

Zhou D, Conrad C, Xia F, Park JS, Payer B, Yin Y, Lauwers GY, Thasler W, Lee JT, Avruch J, Bardeesy N (2009) Mst1 and Mst2 maintain hepatocyte quiescence and suppress hepatocellular carcinoma development through inactivation of the Yap1 oncogene. *Cancer Cell* **16:** 425–438

Zhou D, Medoff BD, Chen L, Li L, Zhang XF, Praskova M, Liu M, Landry A, Blumberg RS, Boussiotis VA, Xavier R, Avruch J (2008) The Nore1B/Mst1 complex restrains antigen receptor-induced proliferation of naive T cells. *Proc Natl Acad Sci USA* **105:** 20321–20326